Helical Resonators for Measuring Dielectric Properties of Materials

W. MEYER

Abstract—A theoretical and practical investigation is given of superconducting helical resonators with quality factors greater than 10^8 which allow the determination of dielectric loss tangents in the frequency range of 0.1 to 5 GHz and below 15 K with high accuracy. The underlying measurement theory is an extension of perturbation theory. They are evaluated for the fields in a shielded multiple quarter-wave helical resonator with a cylindrical dielectric specimen inside the helix. Measurement results on optimized resonators made from superconducting Nb and Nb_3Sn are reported as well as further applications.

Nomenclature

a, b, c, d, l, p	Geometrical resonator parameters defined by Fig. 1.
$c_0 = 2.988 \cdot 10^{10}$ cm^{-1}	Light velocity *in vacuo*.
$f_1 (f_2)$	Resonance frequency of the empty (partially filled) resonator.
$k_B = 6.625 \cdot 10^{34}$ W·s^2	Boltzmann constant.
$k_z = 2\pi/\lambda_z$	Axial propagation constant.
$k_0 = \omega^2 \mu_0 \epsilon_0$	Free-space phase constant.
$k_r = \sqrt{k_z^2 - k_0^2}$	Transversal propagation constant.
l	Electron mean free path.
$p = \omega/k_z$	Axial phase velocity of retarded wave.
r, φ, z	Coordinates of right handed system (Fig. 1).
$v, w = jk_r$	Transversal propagation constant of retarded wave.
A_2, etc.	Amplitude factors.
E, H	Electric (magnetic) field components, indicated by the subscript.
G	Geometric factor.
$H_1^{(2)}$	Bessel function of the third kind and first order (Hankel function).
I_1, I_2	Modified Bessel function of the second kind and of the order indicated by the subscript.
J_1, J_2	Bessel function of the first kind and of the order indicated by the subscript.
K_0, K_1	Bessel function of the second kind and of the order indicated by the subscript.
Q_0	Quality, unloaded.
$Q_1, (Q_2)$	Quality of the empty (partially filled) resonators.
R_A	Measured superconducting surface resistance.
R_{BCS}	Theoretical BCS-surface resistance.
R_{res}	Residual surface resistance.
T	Absolute temperature, in Kelvin (K).
T_c	Critical temperature of superconductivity.
$V_c (V_s)$	Cavity (sample) volume.
V	Improvement factor.
$\beta_1 (\beta_2)$	Input (output) coupling factor of transmission cavity.
δ	Loss angle, in radians.
Δ	Band gap parameter.
$\epsilon_2 = \epsilon_0(\epsilon_2' - j\epsilon_2'')$	Dielectric number.
$\epsilon_0 = 8.854 \cdot 10^{-14}$ A·s·V^{-1}·cm^{-1}	Dielectric constant.
λ_z	Axial wavelength.
λ_{LO}	Superconducting London penetration depth of the electromagnetic field.
$\mu = 1.257 \cdot 10^{-8}$ V·s·A^{-1}·cm^{-1}	Permeability.
ψ	Pitch angle between helix and a circumference.
$\psi^H, (\psi^E)$	Scalar magnetic (electric) potential.

Manuscript received April 8, 1980; revised October 21, 1980

The author is with Philips Research Labs, Vogt-Koelln-Strasse 30, D2000 Hamburg 54, West Germany.

I. Introduction

In connection with recent applications of RF superconductivity, there is growing need for experimental data on microwave low-temperature dielectric properties of materials [1]. Apart from this, dielectric measurements are a powerful tool to gain some insight into molecular structures and mechanisms because of the high measurement sensitivity in the microwave region, especially when using superconducting resonators.

Usually these measurements are accomplished with cavity resonators in the microwave range. Below 6 GHz these cavities become too large for easy handling and consequently not many measurements exist down to 100 MHz, particularly not at low temperatures where we cannot use adjustable condensor plates. For this reason we investigated the properties of helical resonators for measuring

0018-9480/81/0300-0240$00.75

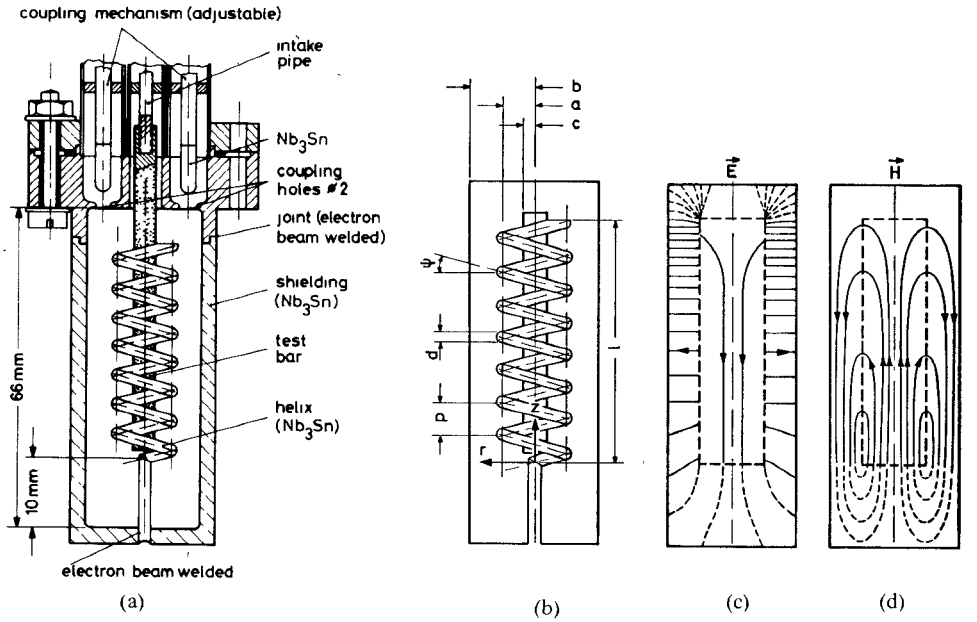

Fig. 1. Helical resonator for a fundamental frequency of 200 MHz ($a=5, b=10, c=3, d=1.5, l=50, p=3$ mm). (a) Constructional details. (b) Definition of geometric parameters. (c) Electric-field configuration. (d) H-field configuration.

dielectric loss because of its small dimensions even at 200 MHz (Fig. 1). The helical resonator is a quarter-wave shorted transmission line in which the center conductor is wound into a helix. This configuration has resonant frequencies approximately at odd multiples of the fundamental and allows measurements to be made within a wide frequency range.

II. Theory of Measurement

Placing a dielectric specimen inside the resonator (Fig. 1), both the electric ($\boldsymbol{E}$) and magnetic ($\boldsymbol{H}$) field configurations change, and quality factor Q and resonance frequency f are altered. The measured shift is related to dielectric constant ϵ_2' and loss tangent $\tan\delta=\epsilon_2''/\epsilon_2'$ (where $\epsilon_2=\epsilon_0(\epsilon_2'-j\epsilon_2'')$) by these formulas [1]:

$$\frac{f_2-f_1}{f_2}=\frac{\epsilon_0\int_{V_s}(\epsilon_1'-\epsilon_2')\boldsymbol{E}_1\boldsymbol{E}_2\,dV_s}{\int_{V_c}(\epsilon_1'\epsilon_0\boldsymbol{E}_1\boldsymbol{E}_2+\mu_1'\mu_0\boldsymbol{H}_1\boldsymbol{H}_2)\,dV_c} \tag{2.1}$$

$$\tan\delta=\frac{1}{2}\left(\frac{\epsilon_1'}{\epsilon_2'}-1\right)\left(\frac{1}{Q_2}-\left(\frac{f_2}{f_1}\right)^2\frac{1}{Q_1}\right)\frac{f_2}{f_2-f_1}\,\frac{K}{\beta_1+\beta_2+1} \tag{2.2}$$

$$K=2\frac{\int_{V_s}\boldsymbol{E}_1\boldsymbol{E}_2\,dV_s}{\int_{V_s}|E_2|^2\,dV_s}\cdot\frac{\int_{V_c}\epsilon_1'\epsilon_0|E_2|^2\,dV_c+\int_{V_s}(\epsilon_2'-\epsilon_1')\epsilon_0|E_2|^2\,dV_s}{\int_{V_c}(\epsilon_1'\epsilon_0\boldsymbol{E}_1\boldsymbol{E}_2+\mu_0\boldsymbol{H}_1\boldsymbol{H}_2)\,dV_c} \tag{2.3}$$

$$K\simeq 1+2\frac{f_1-f_2}{f_2},\qquad \text{for } \boldsymbol{E}_1\equiv\boldsymbol{E}_2. \tag{2.4}$$

(V_s sample volume, V_c resonator volume; subscripts 1 and 2 refer to the empty and partially filled resonator.) The above equations are an extension of the well-known perturbation formalism and only valid for high-Q resonators and small frequency shift and loss tangent

$$\frac{f_2-f_1}{f_2}\leqslant 0.1\qquad \tan\delta\leqslant 0.1\qquad Q_1,Q_2\gg 1. \tag{2.5}$$

Their evaluation affords the knowledge of the field distributions $\boldsymbol{E}_1, \boldsymbol{H}_1$ and $\boldsymbol{E}_2, \boldsymbol{H}_2$.

III. Field Expressions and Quality Factor

We concentrate on the lowest mode ("slow mode") of a concentric line having a tape-helix inner conductor, i.e., the helix is replaced by a fictitious surface conducting only in the helix direction. The wave properties of such a line have been adequately covered in the literature [2]–[9]; we solved the boundary value problem with a concentric dielectric inside the helix in addition. This is done in the Appendix under several assumptions which result in these design restrictions for the actual measurement resonator (all symbols are defined in the Nomenclature and Fig. 1):

$$b/a\geqslant 1.1\qquad a/c\geqslant 1.1 \tag{3.1}$$

$$\cot\psi\gg 1.\qquad (\text{usually } 10\cdots 50) \tag{3.2}$$

$$\lambda_z\gg p \tag{3.3}$$

$$\epsilon_2'\ll\cot\psi. \tag{3.4}$$

The analytical field expressions are listed under equations (A.4), (A.7), (A.11), and sketched in Fig. 1 for the

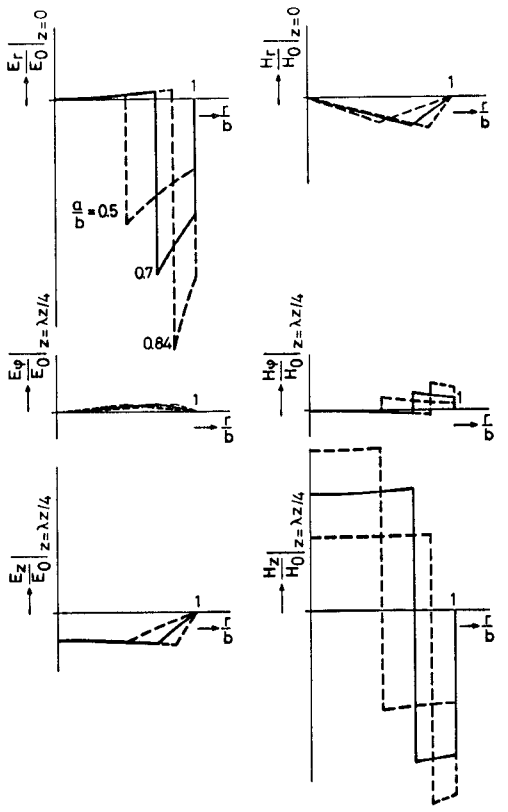

Fig. 2. Normalized maximum field amplitudes at different locations inside the resonator of Fig. 1 $H_0 = A_2(k_0^2/k_0^2 \cot\psi) \simeq A_2 k_z \cot\psi$; $E_0 = A_2(k_z^2/\omega\epsilon_0) \simeq A_2(\sqrt{\mu_0}/\sqrt{\epsilon_0}) k_z \cot\psi$

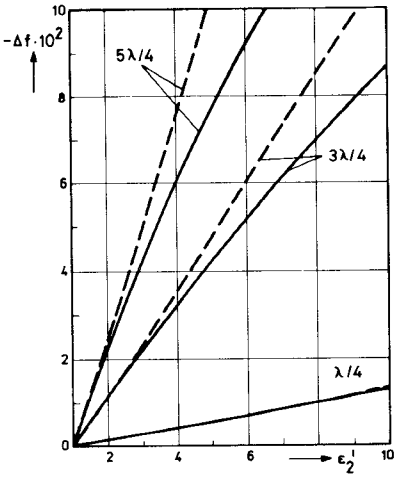

Fig. 3. Frequency shift of helical resonator (Fig. 1) according to (2.1), $\lambda/4$ = fundamental (200 MHz); $3\lambda/4$ = first overtone (600 MHz); $5\lambda/4$ = second overtone (1 GHz); dashed line: approximation with $E_2 = E_1$

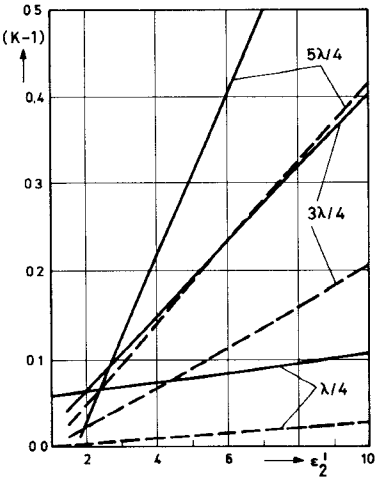

Fig. 4. Correction factor K of helical resonator (Fig. 1) according to (2.3); $\lambda/4$ = fundamental (200 MHz); $3\lambda/4$ = first overtone (600 MHz); $5\lambda/4$ = second overtone (1 GHz). Dashed line: approximation (2.4)

fundamental of the quarter-wave resonator. The qualitative result: most of the energy content located outside the helix — only a very small electric and small magnetic field in the interior — is confirmed by Fig. 2 which shows the maximum normalized field amplitudes at different places within the resonator. The poor electric field concentration at the location of the dielectric is coincident with the general assumption of the perturbation theory that the resonator fields before and after introducing the specimen must be very much alike [10] which corresponds to small frequency shifts. Explicit evaluations of (2.1) with the field expressions derived in the Appendix, for the dimensions according to Fig. 1, are displayed in Fig. 3 which proves the actual frequency pulling sufficiently small for lower ϵ_2'-values. The corresponding correction factor K (2.3), (2.4) is shown in Fig. 4. K considerably deviates from 1; thus its neglect may lead to errors up to 50 or more percent in dissipation measurements.

Besides this, measurement accuracy greatly depends upon the absolute quality factor of the empty resonator; with other words Q has to be maximized. This is impossible with the foregoing field derivation because Q strongly depends on the tangential magnetic fields at the surface of the actual helix, where geometric dimensions have been lost by approaching it by a fictitious surface with nonisotropic conductivity. In fact the evaluation of the current distribution in the helix is quite a complicated problem which has been solved for rectangular helix cross sections only [8], [9]. We adopted the expressions derived in [9] for quadratic helices instead of the wire helix of the referred resonator (Fig. 1), and evaluated the geometric factor defined by

$$G = Q \cdot R_A = \frac{\omega \iiint_V \mu_0 |H|^2 \, dV}{\iint_A |H_a|^2 \, dA}. \tag{3.5}$$

H_a = tangential magnetic field at the inner resonator surface A. The numerical values displayed in Fig. 5 show reasonable coincidence with measured data up to 1 GHz when the initial assumption, axial wavelength $\lambda_z \gg p$, is being violated. The diagram also shows the importance of the wire diameter in the quality factor; optimum conditions over a broad frequency band are achieved with $d/p = b/a = 0.5$. Maximum Q's amount to about 1600 (copper) at

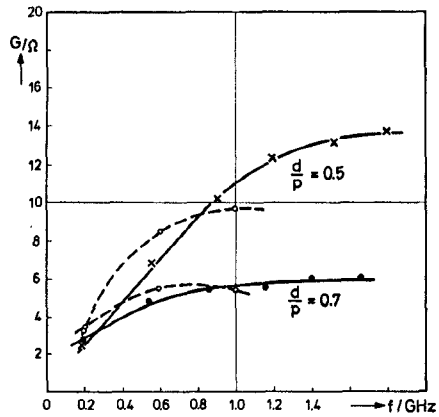

Fig. 5. Geometric factor G of helical resonator (Fig. 1) Solid lines: theoretical values obtained from (3.5); dashed lines: experimental data.

room temperature, and $9\cdot10^8$ (niobium–tin Nb_3Sn) at 2.2 K (see Section IV).

IV. Practical Design and Experimental Setup

Because of the small frequency shift the practical design may start with the design chart Fig. 6, which is the numerical solution of the characteristic equation of the empty helical resonator [7]

$$\left(\frac{k_0 a\cot\psi}{va}\right)^2 = \frac{I_0(va)I_1(vb)\left[I_0(vb)K_0(va)-I_0(va)K_0(vb)\right]}{I_0(vb)I_1(va)\left[I_1(vb)K_1(va)-I_1(va)K_1(vb)\right]}. \quad (4.1)$$

$$v^2=(2\pi/\lambda_z)^2-k_0^2, \qquad k_0^2=\omega^2\mu_0\epsilon_0. \quad (4.2)$$

The chart relates the resonance frequency $f=c_0/\lambda$ ($c_0=$ light velocity *in vacuo*) with the geometrical parameters a, b, ψ, and the axial wavelength λ_z. λ_z in case of the quarter-wave resonator's fundamental is $\lambda_z=4\cdot l$, l being the length of the helix (according to Fig. 1).

Overtones should only be excited in the helix up to a certain limiting frequency when high order "hollow tube" modes begin to propagate with phase velocities greater than light speed. The radial separation constant (i.e., the cutoff frequency) for these modes can be obtained from a characteristic equation similar to (4.1), where the modified Bessel functions are replaced by their normal counterparts. Under condition $\cot\psi \gg 1$ it can be simplified to

$$J_1(k_{r1}b)H_1^{(2)}(k_{r1}a)-J_1(K_{r1}a)H_1^{(2)}(k_{r1}b)=0. \quad (4.3)$$

(4.3) is solved numerically in Fig. 7. For frequencies and dimensions below the curve only the retarded mode can propagate on the line. Different resonators for different purposes were designed following the scopes outlined above: 1) $\lambda/4$-resonators made from Nb and coated with Nb_3Sn for measuring the superconducting surface resistance of these materials; 2) superconducting $\lambda/4$-resonators for measuring the dielectric loss of polymeric materials at cryogenic temperatures; 3) $\lambda/2$-resonators made from copper for determining the dielectric loss (and moisture content in a second step) of organic materials containing water, e.g., tobacco.

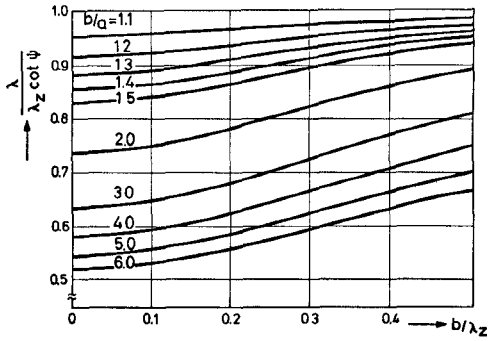

Fig. 6. Design chart of helical resonators: resonant frequency $f=c_0\lambda$ as a function of geometrical parameter a, b, ψ (Fig. 1) and axial wavelength λ_z.

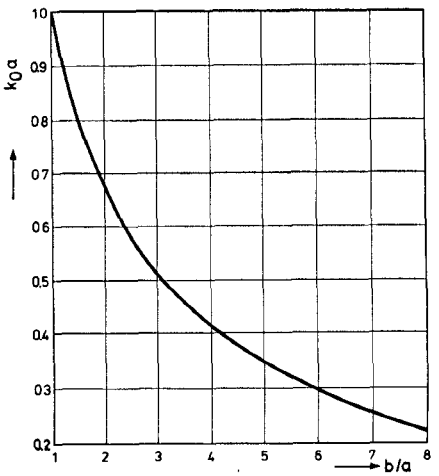

Fig. 7. Cutoff frequency $f_0=c_0k_0/(2\pi)$ of the lowest "hollow tube" mode of the helixresonator (Fig. 1).

A. RF-Superconductivity in Nb and Nb_3Sn

The experimental data on Nb were obtained with resonators sketched in Fig. 1, which after machining were first treated chemically in a HF/HNO_3 solution, then electron beam welded in ultra-high vacuum and afterwards recrystallized at 1300 C. Before each measurement a 5-μm surface layer was removed by an etching process. These resonators showed unloaded Q's of typically $5\cdot10^7$ at 4.2 K, with $9\cdot10^8$ (2.2 K and 190 MHz) at maximum [1]. The Nb_3Sn-resonators were prepared in a CVD-process by tin-diffusion [12], [13] without further surface treatment. The measurements of the frequency and temperature dependence (Figs. 8,9) of superconducting surface resistances can be split into two contributions:

$$R_A(f,T)=R_{BCS}(f,T)+R_{res}(f). \quad (5.1)$$

The theoretical BCS-surface resistance R_{BCS} is roughly decaying exponentially with decreasing temperature and proportional with f^2. The numerical evaluation of the BCS-integrals [14] incorporated in the analytical expression for R_{BCS} affords the knowledge of the critical temperature

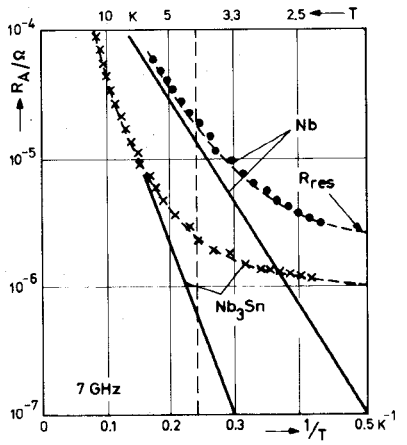

Fig. 8. Temperature dependence of measured superconducting surface resistance R_A of Nb and Nb_3Sn at 7 GHz. Solid lines: theoretical evaluation of the BCS-integrals [14] with the parameters of Table I.

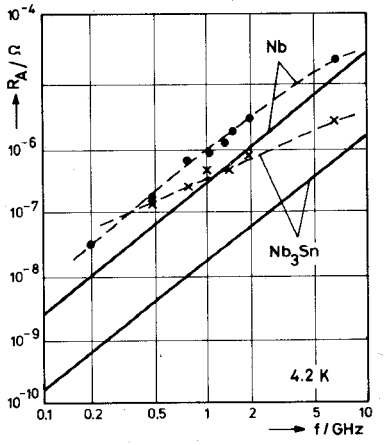

Fig. 9. Frequency dependence of measured superconducting surface resistance R_A of Nb and Nb_3Sn at 4.2 K. Straight lines: theoretical evaluation of the BCS-integrals [14] with the parameters of Table I.

TABLE I
BCS PARAMETERS FOR Nb_3Sn [13] AND Nb [14]

	T_c/K	Δ/k_BT_c	ξ_0/Å	λ_{LO}/Å	1/Å
NB	9.25	1.85	390	320	350
Nb_3Sn	18.0	1.80	125	390	18

T_c and band gap parameter Δ as well as the electronical parameters for Nb and Nb_3Sn: electron mean free path 1, London penetration depth λ_{LO}, and coherence length ξ_0, which are compiled in Table I.

The deviations between theoretical and measured curves (Figs. 8,9) are due to the residual surface R_{res} which is independent from temperature and is closely related to the state of the surface (smoothness, contaminations, etc). Its physical origin is not quite well understood yet; presently the most feasible microscopic model is based on phonon exchange among traps in the surface layer of the metal [15], [16].

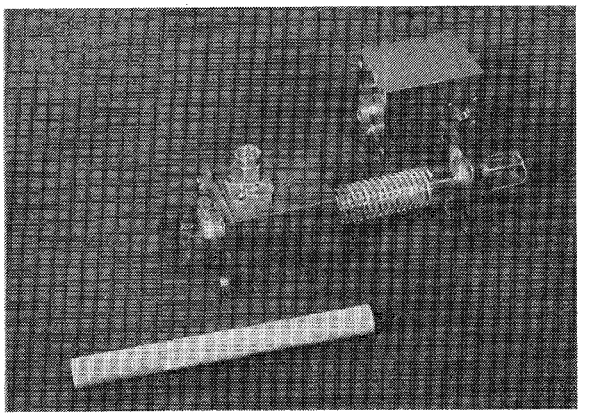

Fig. 10. Photograph of $\lambda/2$-helical resonator as sensing head for moisture determination of cigarettes.

B. Dielectric Measurements at Low Temperatures

According to (2.2) very low loss tangents can be determined with high-Q resonators. The quantities of (2.2), resonance frequency f, loaded quality factor Q, and coupling coefficients β, are obtained in a high-precision test assembly, which is described in detail elsewhere [17]. It consists of the transmission type resonator, which is the frequency determining element in a closed loop, in series with phase shifter, broad-band transistor amplifier, and a p-i-n modulator which interrupts the stationary oscillation being possible under appropriate phase conditions and sufficient amplification. The quality factor is obtained from the exponential decay of the resonator power envelope, the coupling factors are determined by measuring the incident and transmitted powers during steady-state, and the resonance frequency is measured with a microwave counter. Measurement errors do not exceed ± 2 percent for Q's greater than 10^4; therewith the relative error of $\tan\delta$ measurement generally amounts to less than 5 percent for $\tan\delta \geqslant 5 \cdot 10^{-7}$. Extensive investigations on various polymers and glasses using this measurement equipment have been published elsewhere [18]–[20] and go beyond the scope of this paper.

C. Applicator for Moisture Determination

Microwave resonator techniques are used in testing material properties which are related to its dielectric properties, e.g., measuring the water content in tobacco [21], [22]. As a sensing head (or applicator) for cigarettes a $\lambda/2$-helical resonator was developed (Fig. 10). The helix is wound around a silica tube which contains the specimen. It has no connection with the shielding and is excited by a capacitive probe at one end of the helix. The resonator can be used from 500 MHz up to 5 GHz when higher order modes begin to propagate at the line. The onset of these modes is clearly visible from the discontinuity in the quality factor of the empty resonator and in the frequency shift after insertion of a specimen (Fig. 11). This resonator was used for determining the loss tangent of moist tobacco over a wide-frequency range (Fig. 11(c)), but of course is suit-

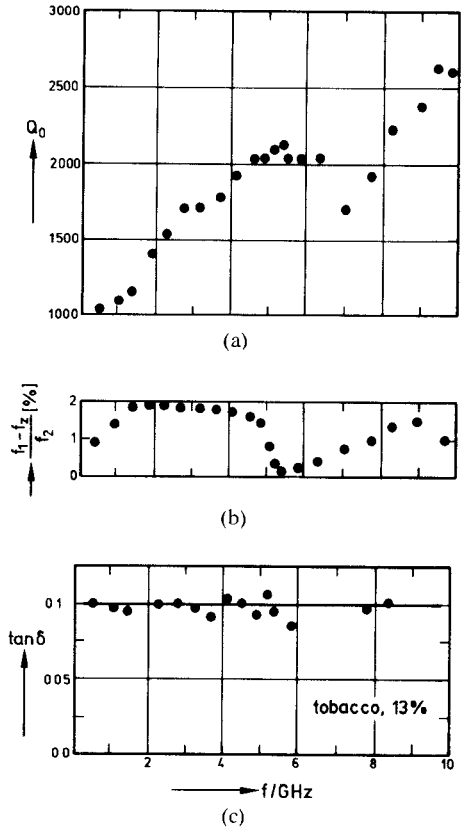

Fig. 11. (a) Quality factor Q_0 of the helical resonator (Fig. 10). (b) Frequency shift of the helical resonator (Fig. 10) after insertion of a teflon rod with $\epsilon'_2=2.1$. (c) Loss tangent of cigarettes with a moisture content of 13 percent.

able for any kind of materials which undergo microwave absorptions, e.g., polar fluids.

V. Conclusion

The helical resonator as a measuring device for material properties has been investigated and measuring results for superconductors and dielectrics have been presented. This type of resonator has the advantage of small dimensions compared to the wavelength and quite high quality factors. It fits well into the intermediate region between the higher megahertz and lower gigahertz range, where cavities grow too big for easy handling.

Appendix

Derivation of Field Expressions for a Helical Conductor Surrounded by a Coaxial Conductive Cylinder with a Coaxial Dielectric Partially Filling the Interior

As there is always an H-field at the center axis at $r=0$, the fields can be shown to belong to a single φ-independent mode at low frequencies [8]. With regard to the described application as a measurement resonator we are only concerned with this slow mode wave, i.e., the axial phase velocity $p=\omega/k_z$ is smaller than the light velocity and the transversal propagation constant $k_r=-jv=\sqrt{k_0^2-k_z^2}$ (all symbols are defined in the glossary) is imaginary. Therefore we use the modified Bessel function of the second kind $K_0(vr)$ in the scalar potentials ψ^H, ψ^E, which with respect to the three different regions of the line are as follows:

Region 1 $(0<r\leqslant c)$

$$\psi_1^E=A_2 I_0(wr)e^{\pm jk_z z}$$
$$\psi_1^H=B_2 I_0(wr)e^{\pm jk_z z}$$

Region 2 $(c\leqslant r\leqslant a)$

$$\psi_2^E=\left[C_{12}I_0(vr)+C_{22}K_0(vr)\right]e^{\pm jk_z z}$$
$$\psi_2^H=\left[D_{12}I_0(vr)+D_{22}K_0(vr)\right]e^{\pm jk_z z}$$

Region 3 $(a\leqslant r\leqslant b)$

$$\psi_3^E=\left[F_1 I_0(vr)+F_2 K_0(vr)\right]e^{\pm jk_z z}$$
$$\psi_3^H=\left[G_1 I_0(vr)+G_2 K_0(vr)\right]e^{\pm jk_z z} \qquad \text{(A.1)}$$

with the transversal propagation constants v and w inside and outside the dielectric

$$v^2=k_z^2-k_0^2 \qquad k_0^2=\omega^2\mu_0\epsilon_0$$
$$w^2=k_z^2-k_1^2 \qquad k_1^2=\omega^2\mu_0\epsilon'_2\epsilon_0. \qquad \text{(A.2)}$$

With the general relations between the scalar potentials and the fields

$$E_r=\frac{1}{j\omega\epsilon}\frac{\partial^2\psi^E}{\partial r\partial z} \qquad H_r=\frac{1}{j\omega\mu_0}\frac{\partial^2\psi^H}{\partial r\partial z}$$
$$E_\varphi=\frac{\partial\psi^H}{\partial r} \qquad H_\varphi=\frac{\partial\psi^E}{\partial r}$$
$$E_z=\frac{1}{j\omega\epsilon}\left(\frac{\partial^2}{\partial z^2}+k_0^2\right)\psi^E \qquad H_z=\frac{1}{j\omega\mu_0}\left(\frac{\partial^2}{\partial z}+k_0^2\right)\psi^H \qquad \text{(A.3)}$$

and regarding the shorted end of the helix as an electrical shorting termination only [9], we end up with the following expressions for the field components.

Region 1 $(0<r\leqslant c)$

$$E_{r1}=A_2\frac{wk_z}{\omega\epsilon_0\epsilon'_2}I_1(wr)\cos(k_z z)$$
$$E_{\varphi 1}=B_2 wI_1(wr)\sin(k_z z)$$
$$E_{z1}=A_2\frac{w^2}{\omega\epsilon_0\epsilon'_2}I_0(wr)\sin(k_z z)$$
$$H_{r1}=-jB_2\frac{wk_z}{\omega\mu_0}I_1(wr)\cos(k_z z)$$
$$H_{\varphi 1}=-jA_2 wI_1(wr)\sin(k_z z)$$
$$H_{z1}=jB_2\frac{w^2}{\omega\mu_0}I_0(wr)\sin(k_z z).$$

Region 2 ($c \leq r \leq a$)

$$E_{r2} = \frac{vk_z}{\omega\epsilon_0}\left[C_{12}I_1(vr) - C_{22}K_1(vr)\right]\cos(k_z z)$$

$$E_{\varphi 2} = v\left[D_{12}I_1(vr) - D_{22}K_1(vr)\right]\sin(k_z z)$$

$$E_{z2} = \frac{v^2}{\omega\epsilon_0}\left[C_{12}I_0(vr) + C_{22}K_0(vr)\right]\sin(k_z z)$$

$$H_{r2} = -j\frac{vk_z}{\omega\mu_0}\left[D_{12}I_1(vr) - D_{22}K_1(vr)\right]\cos(k_z z)$$

$$H_{\varphi 2} = -jv\left[C_{12}I_1(vr) - C_{22}K_1(vr)\right]\sin(k_z z)$$

$$H_{z2} = j\frac{v^2}{\omega\mu_0}\left[D_{12}I_0(vr) + D_{22}K_0(vr)\right]\sin(k_z z).$$

Region 3 ($a \leq r \leq b$)

$$E_{r3} = \frac{vk_z}{\omega\epsilon_0}\left[F_1I_1(vr) - F_2K_1(vr)\right]\cos(k_z z)$$

$$E_{\varphi 3} = v\left[G_1I_1(vr) - G_2K_1(vr)\right]\sin(k_z z)$$

$$E_{z3} = -\frac{v^2}{\omega\epsilon_0}\left[F_1I_0(vr) + F_2K_0(vr)\right]\sin(k_z z)$$

$$H_{r3} = -j\frac{vk_z}{\omega\mu_0}\left[G_1I_1(vr) - G_2K_1(vr)\right]\cos(k_z z)$$

$$H_{\varphi 3} = -jv\left[F_1I_1(vr) - F_2K_1(vr)\right]\sin(k_z z)$$

$$H_{z3} = j\frac{v^2}{\omega\mu_0}\left[G_1I_0(vr) + G_2K_0(vr)\right]\sin(k_z z). \quad \text{(A.4)}$$

B_2, C_{12}, C_{22}, D_{12}, D_{22}, F_1, F_2, G_1, and G_2 are amplitude factors, which together with the propagation constants v, w, and k_z can be evaluated by these twelve boundary conditions (the subscripts refer to coordinates in the respective regions).

At $r=c$

$$E_{\varphi 1} = E_{\varphi 2} \qquad E_{z1} = E_{z2} \qquad H_{\varphi 1} = H_{\varphi 2} \qquad H_{z1} = H_{z2}.$$

At $r=b$

$$E_{\varphi 3} = 0 \qquad E_{z3} = 0. \quad \text{(A.5)}$$

At $r=a$, *The Fictitious Helix Surface*

$$E_{\varphi 2} = E_{\varphi 3} \qquad E_{z2} = E_{z3}$$

$$E_{\varphi 2}\cos\psi + E_{z2}\sin\psi = 0$$

$$H_{\varphi 1}\cos\psi + H_{z1}\sin\psi = H_{\varphi 3}\cos\psi + H_{z3}\sin\psi. \quad \text{(A.6)}$$

The solution of this set of equations is an elaborate problem, quite impossible analytically without suitable assumptions. We assume identical propagation constants

$$v \simeq w \simeq \sqrt{\epsilon_0\mu_0}\cot\psi \quad \text{(A.7)}$$

which is appropriate in case of small dielectric constants

$$\epsilon_2' \ll \cot^2\psi \quad \text{(A.8)}$$

or slight perturbations where only a small portion of the resonator's energy content is concentrated in the specimen.

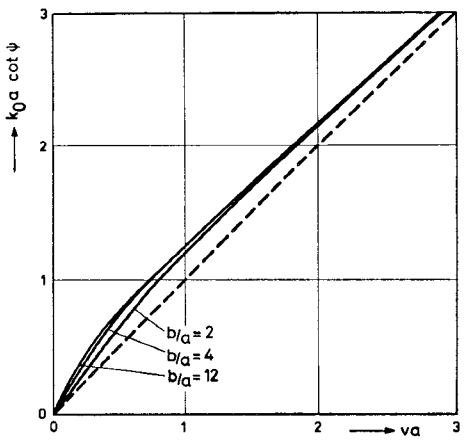

Fig. 12. Transversal phase constant v of the empty helix resonator (Fig. 1); solution of the characteristic equation (4.1)

In this case the resonance frequency is mainly determined by v (A.2), which can be obtained from the characteristic equation of the empty resonator (4.1). Its evaluation (Fig. 12) results in $v \simeq k_0 \cdot \cot\psi$ for $va > 1$, i.e., $k_0 \ll v$ for small pitch angles ψ. This condition together with (A.2) leads to the approximations $v \simeq k_z$ and

$$k_0 \simeq k_z/\cot\psi. \quad \text{(A.9)}$$

Combination of (A.9) with (A.2) yields

$$w \simeq v\sqrt{\left(1-\epsilon_2'/\cot^2\psi\right)/\left(1-1/\cot^2\psi\right)} \quad \text{(A.10)}$$

and, with condition (A.8), the desired relation (A.7). Herewith the amplitude factors of (A.4) can be obtained by analytical solution of (A.4)–(A.6)

$$C_{12} = A_2\frac{\frac{1}{\epsilon_2'}I_0(vc)K_1(vc) + I_1(vc)K_0(vc)}{I_0(vc)K_1(vc) + I_1(vc)K_0(vc)}$$

$$C_{22} = -A_2\frac{\left(1-\frac{1}{\epsilon_2'}\right)I_0(vc)I_1(vc)}{I_0(vc)K_1(vc) + I_1(vc)K_0(vc)}$$

$$B_2 = D_{12} = \frac{1}{\omega\epsilon_0}\frac{1}{\cot\psi}\frac{1}{I_1(va)}\left[C_{12}I_0(va) + C_{22}K_0(va)\right]$$

$$D_{22} = 0$$

$$F_1 = K_0(vb)\frac{C_{12}I_0(va) + C_{22}K_0(va)}{I_0(va)K_0(vb) - I_0(vb)K_0(va)}$$

$$F_2 = -F_1\frac{I_0(vb)}{K_0(vb)}$$

$$G_1 = \frac{v}{\omega\epsilon_0}\frac{1}{\cot\psi}K_1(vb)\frac{C_{12}I_0(va) + C_{22}K_0(va)}{I_1(va)K_1(vb) - I_1(vb)K_1(va)}$$

$$G_2 = G_1\frac{I_1(vb)}{K_1(vb)}. \quad \text{(A.11)}$$

With equations (A.4), (A.7), and (A.11) the field components are determined in terms of a common amplitude factor A_2 dependent upon the excitation or energy content of the resonator. For completeness it should be mentioned

that all field components are multiplied by $\exp(j\omega t)$ for harmonic excitation. The above field expressions convert into the well-known fields of the shielded line without dielectric [4], [7], [8] for $\epsilon_2' = 1$.

References

[1] W. Meyer, "Dielectric measurements on polymeric materials by using superconducting microwave resonators," *IEEE Trans. Microwave Theory Tech.*, vol. 25, pp. 1092–1099, 1977.

[2] H. Kaden, "Eine allgemeine Theorie des Wendelleiters," *Arch. Elek. Übertragung.*, vol. AEÜ-5, pp. 534–538, 1951.

[3] W. Sichak, "Coaxial line with helical inner conductor," *Proc. IRE*, pp. 1315–1319, 1953.

[4] W. Pöschl, "Wellenfortpflanzung längs einer Wendel mit zylindrischem Aussenleiter," *Arch. Elek. Übertragung.*, vol. AEÜ-7, pp. 518–522, 1953.

[5] G. Piefke, "Reflexion in Wendelleitungen bei Änderung der Wendelsteigung," *Arch. Elek. Übertragung.* vol. AEÜ-9, pp. 369–374, 1955.

[6] L. Stark, "Lower modes of a concentric line having a helical inner conductor," *J. Appl. Phys.*, vol. 25, pp. 1155–1162, 1954.

[7] J. H. Bryant, "Some wave properties of helical conductors," *Electr. Commun.*, vol. 31, pp. 50–56, 1954.

[8] D. J. Miley, "Field analysis of helical resonators with constant-bandwidth filter application," *IEEE Trans. Parts, Mater., Packag.*, vol. PMP-5, pp. 127–128, 1969.

[9] G Rotter, "Die Berechnung der Kenngrössen von Wendelleitungs-resonatoren," *Arch. Elek. Übertragung.*, vol. AEÜ-25, pp. 25–31, 1971.

[10] R. A. Waldron, "Perturbation theory of resonant cavities," *Proc. Inst. Elec. Eng.*, pp. 272–274, 1960.

[11] F. Horner *et al.*, "Resonance methods of dielectric measurements at centimetre wavelength," *Proc. Inst. Elec. Eng.*, vol. 89, pt. III, pp. 53–68, 1946.

[12] P. Kneisel *et al.*, "Nb_3Sn for superconducting RF-activities," *Adv. Cryogenic Eng.*, vol. 22, pp. 341–346, 1977.

[13] P. Kneisel *et al.*, "Properties of superconducting Nb_3Sn for hf-cavities," in *Proc. 1977 int. Cryogenic Materials Conf.*, (Boulder, CO), Aug. 2–5, 1977.

[14] E. Voges and V. K. Petermann, "Losses in superconducting coaxial transmission lines," *Arch. Elek. Übertragung.*, vol. AEÜ-27, pp. 384–388, 1973.

[15] J. Halbritter, "On interfacial tunneling of superconducting surfaces," *Phys. Lett.*, vol. 43A, pp. 309–310, 1973.

[16] J. Halbritter, "On rf-residual losses and phonon generation," *IEEE Trans. Magn.*, vol. MAG-II, pp. 427–430, 1975.

[17] W. Meyer, "High sensitivity dielectric loss measurements by using superconducting microwave resonators in an oscillator loop," *Electron. Lett.* vol. 13, pp. 7–8, 1977.

[18] W. Meyer, "New materials for superconductive communication cables," *IEEE Trans. Commun.*, vol. 25, pp. 449–458, 1978.

[19] J. le G. Gilchrist and W. Meyer, "Dielectric loss spectrum of hydrated vitreous silica," in *Advances in Cryogenic Engineering* vol. 24, K. D. Timmerhaus *et al.*, Eds. New York: Plenum, 1978.

[20] W. Meyer, "Variation of dielectric microwave losses in PE as the result of different sample treatments," in *Nonmetallic Materials and Composites at Low Temperatures*, A. F. Clark *et al.*, Eds. New York: Plenum, 1979.

[21] A. Kraszewski, "Microwave instrumentation for moisture content measurement," *J. Microwave Power*, vol. 8, pp. 323–335, 1973.

[22] W. Meyer and W. Schilz, "Microwave absorption by water in organic materials," *Dielectric Materials, Measurements and Applications* Inst. Elec. Eng. Publ. 177, 1979, pp. 215–219.

Measurement of Losses in Noise-Matching Networks

ERIC W. STRID

Abstract—**The noise contribution of an input-matching network to a low-noise amplifier is equal to the inverse of the network's available gain. The available gain of various networks at 4 GHz was computed from high-accuracy *S*-parameter measurements. The available gain of a typical tuner was experimentally found to be a strong function of its tuning, which shows that "back-to-back" measurements of two tuners to obtain the loss of each tuner can be inaccurate. Measurement of the available gain of an amplifier's input-matching circuit is shown to give quick insight into its minimum noise contribution before the actual amplifier stage is built.**

I. Introduction

SOME APPLICATIONS of microwave amplifiers require squeezing out every bit of low-noise performance from an active device. One such application is a satellite earth station low-noise amplifier, whose contribution to system operating noise temperature is relatively large due to the low equivalent temperature of the antenna [1]. Development of such amplifiers requires selection of the best active devices, circuit materials, and techniques.

The noise of active two-ports is usually characterized with an impedance-substitution setup such as that shown in Fig. 1 [2]. Small losses in the components between the noise generator and the device under test (DUT) contribute directly to the total noise figure, and the accuracy to which this loss is known contributes directly to the accuracy of the noise-figure measurement. In current practice, the losses of typical input circuits used in microwave-transistor noise-test setups are in the range of 0.1–1 dB. This range is normally much greater than the uncertainty in the calibration of the noise source. Because this uncertainty leads to inaccurate noise data for the device, especially F_{min} data,

Manuscript received June 3, 1980; revised October 28, 1980.

The author was with Farinon Transmission Systems, San Carlos, CA. He is now with Applied Research Group, Tektronix Laboratories, Tektronix, Inc., Beaverton, OR 97077.

0018-9480/81/0300-0247$00.75 ©1981 IEEE